

## Summer Cooling Driven by Large Volcanic Eruptions over the Tibetan Plateau

JIANPING DUAN,<sup>a,b</sup> LUN LI,<sup>c</sup> ZHUGUO MA,<sup>a</sup> JAN ESPER,<sup>d</sup> ULF BÜNTGEN,<sup>e</sup> ELENA XOPLAKI,<sup>f</sup>  
DUJUAN ZHANG,<sup>g</sup> LILY WANG,<sup>h</sup> HONG YIN,<sup>i</sup> AND JÜRIG LUTERBACHER<sup>f,j</sup>

<sup>a</sup> Key Laboratory of Regional Climate-Environment for Temperate East Asia,  
Institute of Atmospheric Physics, Chinese Academy of Sciences, Beijing, China

<sup>b</sup> State Key Laboratory of Vegetation and Environmental Change, Institute of Botany,  
Chinese Academy of Sciences, Beijing, China

<sup>c</sup> Chinese Academy of Meteorological Sciences, Beijing, China

<sup>d</sup> Department of Geography, Johannes Gutenberg University, Mainz, Germany

<sup>e</sup> Department of Geography, University of Cambridge, Cambridge, United Kingdom

<sup>f</sup> Department of Geography, Justus Liebig University of Giessen, Giessen, Germany

<sup>g</sup> Department of Geographic Science, Shanxi Normal University, Linfen, China

<sup>h</sup> Institute of Geographic Sciences and Natural Resources Research, Chinese  
Academy of Sciences, Beijing, China

<sup>i</sup> National Climate Center, China Meteorological Administration, Beijing, China

<sup>j</sup> Centre of International Development and Environmental Research, Justus Liebig  
University of Giessen, Giessen, Germany

(Manuscript received 4 October 2017, in final form 10 September 2018)


### ABSTRACT

Large volcanic eruptions may cause abrupt summer cooling over large parts of the globe. However, no comparable imprint has been found on the Tibetan Plateau (TP). Here, we introduce a 400-yr-long temperature-sensitive network of 17 tree-ring maximum latewood density sites from the TP that demonstrates that the effects of tropical eruptions on the TP are generally greater than those of extratropical eruptions. Moreover, we found that large tropical eruptions accompanied by subsequent El Niño events caused less summer cooling than those that occurred without El Niño association. Superposed epoch analysis (SEA) based on 27 events, including 14 tropical eruptions and 13 extratropical eruptions, shows that the summer cooling driven by extratropical eruptions is insignificant on the TP, while significant summer temperature decreases occur subsequent to tropical eruptions. Further analysis of the TP August–September temperature responses reveals a significant postvolcanic cooling only when no El Niño event occurred. However, there is no such cooling for all other situations, that is, tropical eruptions together with a subsequent El Niño event, as well as extratropical eruptions regardless of the occurrence of an El Niño event. The averaged August–September temperature deviation ( $T_{\text{dev}}$ ) following 10 large tropical eruptions without a subsequent El Niño event is up to  $-0.48^{\circ} \pm 0.19^{\circ}\text{C}$  (with respect to the preceding 5-yr mean), whereas the temperature deviation following 4 large tropical eruptions with an El Niño association is approximately  $0.23^{\circ} \pm 0.16^{\circ}\text{C}$ . These results indicate a mitigation effect of El Niño events on the TP temperature response to large tropical eruptions. The possible mechanism is that El Niño events can weaken the Indian summer monsoon with a subsequent decrease in rainfall and cooling effect, which may lead to a relatively high temperature on the TP, one of the regions affected by the Indian summer monsoon.

### 1. Introduction

Volcanic eruptions are a major natural driver of climate variability (Robock 2000). Sulfate aerosols from large volcanic eruptions that are injected into the

stratosphere can shield Earth's surface from incoming solar radiation, causing regional or global surface cooling (Briffa et al. 1998; Sigl et al. 2015; Stoffel et al. 2015; Luterbacher and Pfister 2015; Büntgen et al. 2016; Schneider et al. 2017; Esper et al. 2015). One well-known case of this phenomenon is the eruption of Tambora in April 1815, which led to “the year without a summer” in 1816 in western Europe and northern North America (Stothers 1984; Oppenheimer 2003; Luterbacher and Pfister 2015; Luterbacher et al. 2016). Following large

 Denotes content that is immediately available upon publication as open access.

Corresponding author: Jianping Duan, duanjp@tea.ac.cn

DOI: 10.1175/JCLI-D-17-0664.1

© 2018 American Meteorological Society. For information regarding reuse of this content and general copyright information, consult the AMS Copyright Policy ([www.ametsoc.org/PUBSReuseLicenses](http://www.ametsoc.org/PUBSReuseLicenses)).

volcanic eruptions, exceptionally low tree-ring growths across large areas of the northern mid–high latitudes have been documented (Briffa et al. 1998; Sigl et al. 2015). However, in contrast to the evidences identified in the northern mid–high latitudes, no comparable imprint of some large eruptions (e.g., the Tambora eruption in 1815) can be found on the Tibetan Plateau (TP; Bräuning and Mantwill 2004; Duan and Zhang 2014; Duan et al. 2017). The cause of this subdued volcanic effect on the TP is still unclear.

The TP is the highest and largest plateau in the world and often responds more sensitively to climate change than do other areas at the same latitude (Duan et al. 2015). Surface temperature changes in this unique geographic unit have strong effects on both the climate and ecosystems of the Asian continent and can even impact much larger areas (Yao et al. 2012; Duan et al. 2015). However, the uniqueness of this region and the complexity of the interactions between climatic drivers on the TP make it difficult to fully understand the long-term mechanisms of climate change on the TP (Sato 2009). For the interannual temperature variability, in addition to the external forcing (i.e., volcanic eruptions), internal phenomenon is also an important driving factor. For example, the contribution of ENSO to global air temperature variations over the past 150 years is 10%–30% (Privalsky and Jensen 1995). The influence of ENSO on climate was also reported on the TP and in surrounding areas. One of the most important effects is that ENSO has a direct influence on the Indian monsoon (Kumar et al. 1999). Moreover, a potential link between temperature variations on the TP and ENSO was also reported (Yin et al. 2000; Wang et al. 2003). However, most previous studies performed on the TP are based on relatively short instrumental records, and the influence of the interaction between external volcanic forcings and internal ENSO variations on the interannual temperature variability over the TP has not been explored. Here, we put forward a hypothesis that ENSO influences the interannual temperature variability on the TP by impacting the strength of the Indian monsoon, which in turn mediates the response of the TP temperature to volcanic eruptions. The identification and evaluation of climatic extremes from periods before the mid-twentieth century require high-quality proxy archives (Cook et al. 2013).

Annually resolved tree-ring data are important sources for the assessment of past summer cooling following strong volcanic eruptions (D'Arrigo et al. 2009; Anchukaitis et al. 2010; Esper et al. 2013a; Sigl et al. 2015). Compared to the commonly used tree-ring width (TRW), measurements of maximum latewood density (MXD) are more sensitive to summer temperature variability and, likely, even to light

availability (Stine and Huybers 2014; Esper et al. 2015; Duan et al. 2017). Moreover, the MXD is less biased by biological memory effects or growth-inertia characteristics compared to the TRW (Frank et al. 2007; Esper et al. 2013b; Büntgen et al. 2015). The growth of the tree-ring MXD is usually controlled by temperature conditions in the growing season or late summer (Briffa et al. 1988; Schweingruber et al. 1991). This is the important period for tracheid cell wall thickening. Favorable temperatures in summer are conducive to photosynthesis and contribute to latewood cell wall thickening and the production of higher latewood density. Contrarily, cool summers can result in low latewood density. This relationship has also been demonstrated in previous TP MXD studies (Bräuning and Mantwill 2004; Fan et al. 2009; Wang et al. 2010; Duan et al. 2010, 2017; Duan and Zhang 2014). Therefore, summer cooling resulting from volcanic eruptions can also lead to an MXD decrease.

Here, we estimate the magnitude of cooling after large volcanic eruptions since 1620 over the TP based on a temperature-sensitive network of 17 tree-ring MXD sites. Furthermore, we explore the potential causes of the unobvious imprints of large volcanic eruptions on the TP compared to those documented in other regions. Especially, we will identify the cooling effect driven by external volcanic forcing with consideration of the internal ENSO influence. The structure of this paper is as follows: In section 2, the materials and methods used in this study are described briefly. Section 3 presents the main results obtained from this study. Section 4 focuses on a discussion of the results and possible mechanisms. Section 5 summarizes the conclusion.

## 2. Materials and methods

### a. Tree-ring MXD data

Tree-ring MXD data were derived from old-growth Balfour spruce (*Picea likiangensis* var. *balfouriana*) trees at 17 high-elevation sites on southeastern TP (Fig. 1). For tree-ring-based climate reconstructions, tree-ring sampling sites without any natural or human disturbance (e.g., fire, pathogen outbreaks, and grazing) need to be chosen to guarantee that the pure climatic signal can be extracted from the collected tree-ring samples. To identify these disturbances, in addition to traces left on trees (e.g., fire scarring), detailed inquiries or investigations on the associations from the local residents, forestry bureaus, or document records can also be important means of obtaining information. Moreover, the analysis of metadata (e.g., the coherence among trees and coherence among chronologies/sites) can also be an approach to identifying pathogen disturbances in forests. In this study, all sampling sites were without any evidence or record of

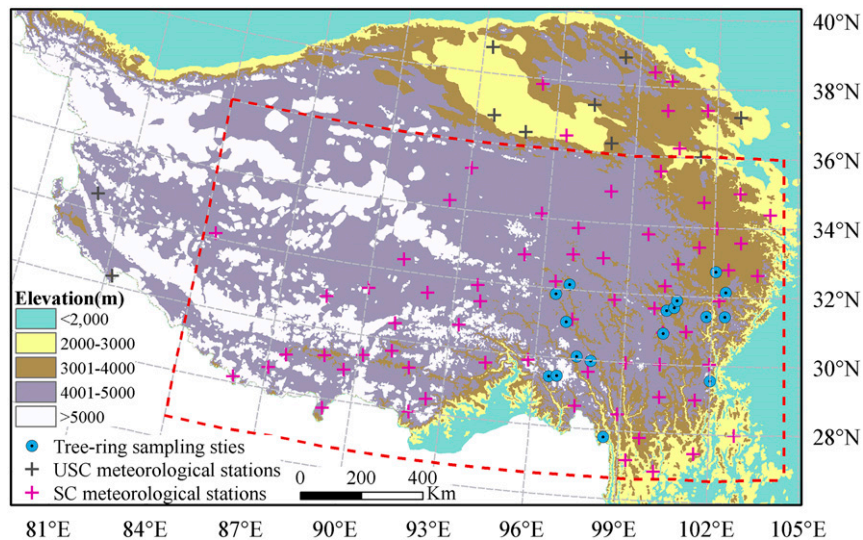


FIG. 1. Map showing the locations of tree-ring sites and meteorological stations. Magenta and dark gray crosses mark the meteorological stations for which the August–September  $T_{dev}$  correlates significantly ( $P < 0.05$ ) and insignificantly ( $P > 0.05$ ) with the regional MXD\_GD series, respectively. The red-dashed-line box denotes the spatial scope of the 62 meteorological stations for which the August–September  $T_{dev}$  correlates significantly ( $P < 0.05$ ) with the MXD\_GD series. Detailed information about the correlations is provided in the materials and methods section.

natural or human disturbances that might have impacted tree growth. The tree-ring density of the collected samples was measured using the X-ray method according to standard practices (Schweingruber et al. 1988; Duan et al. 2010). Considering that ring dating after densitometric analysis might be problematic because some cores are unavoidably broken during the process of sugar and resin extraction and sample sectioning, we performed ring-width measurements and cross dating before densitometric analysis. The measured ring-density data were dated based on tree-ring width cross dating, and were verified with thin wood sections when inconsistencies appeared. The quality of densitometric cross dating was tested using the quality control and dating check of tree-ring measurements (named as COFECHA) program (Holmes 1983). Thus, although the sizes of the samples vary with time, the quality of cross dating is guaranteed. A total of 739 measured MXD sequences were dated to the corresponding calendar years, and the longest series reaches back to 1375 (Fig. 2). Because the number of samples decreased back in time, the effect on the chronology signal strength was evaluated using the expressed population signal (EPS; Wigley et al. 1984). The reliable period of the regional composite growth deviation (MXD\_GD) series was determined considering the criterion of  $EPS > 0.85$ , calculated based on the regional MXD raw chronology using autoregressive standardization (ARSTAN) software (Cook and Krusic 2005). The resulting reliable period starts in

1620, with the smallest sample size of 39 cores, and ends in 2014 (Fig. 2). We developed MXD\_GD based on the network comprising 739 MXD measurement series from 17 sites on the TP.

The regional MXD\_GD series was calculated as the MXD deviation for each year relative to the preceding 5-yr mean:

$$\text{MXD\_GD}_i(\%) = (\text{MXD}_i - \text{MXD}_{i-1:i-5}) / \text{MXD}_{i-1:i-5},$$

with  $\text{MXD}_i$  representing the MXD value in year  $i$  and  $\text{MXD}_{i-1:i-5}$  corresponding to the mean values from year  $i - 1$  to year  $i - 5$ . This calculation was applied for each year and all MXD measurement series. The final regional MXD\_GD series was obtained by averaging all 739 individual MXD\_GD series. The MXD\_GD series is designed to examine the relative growth change, also referred to as the abrupt growth change, of the tree-ring MXD following a volcanic eruption. This approach has also been used to explore the response of other tree-ring parameters, such as tree-ring widths, to extreme climate/disturbance events (Schweingruber et al. 1990). The formula can provide quantitative evaluation of growth responses of the tree-ring MXD to volcanic eruptions. Based on this evaluation, the quantitative magnitude of temperature changes triggered by these events can be calculated. In this study, we chose a 5-yr window (i.e., relative to the preceding 5-yr mean) and tried windows from 1–4 years. We found that there is little

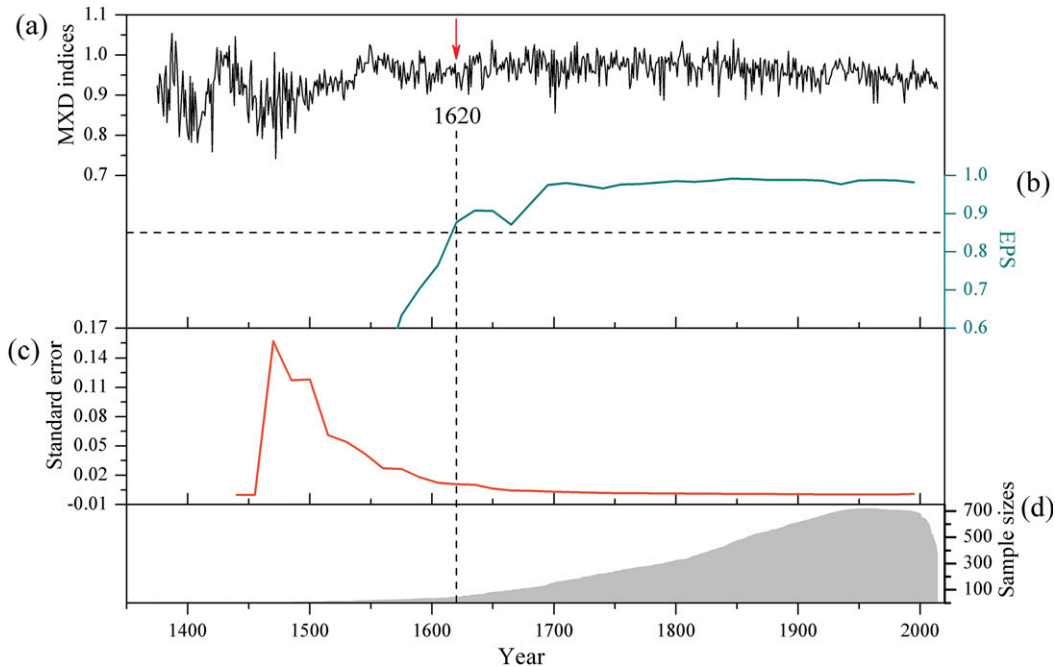


FIG. 2. Regional tree-ring (a) MXD raw chronology with the (b) EPS, (c) standard error, and (d) sample size. The pink arrow indicates the starting year for which the EPS was greater than 0.85.

difference, and the 5-yr window is the best for capturing the temperature signal (figure not shown).

#### b. Climatic data

Homogeneous monthly temperature data from 79 meteorological stations (Duan et al. 2015) at elevations above 2000 m MSL were used in this study (Fig. 1). The record length varies among stations, but each includes at least 36 years from 1979 to 2014. The gridded land surface air temperature data used in this study are from the Climatic Research Unit Global Temperature, version 4.3 (CRUTEM4.3), and have a spatial resolution of  $5^{\circ}$  by  $5^{\circ}$  starting in 1850 (Jones et al. 2012).

#### c. Growth–climate relationships

The growth–climate response relationships of the regional MXD\_GD series were analyzed against monthly temperature data from April–September both for individual station records and at different regional scales. To maintain consistency with the calculated MXD\_GD series, observational monthly temperature series were also calculated as temperature deviations ( $T_{\text{dev}}$ ) with respect to the preceding 5-yr mean.

#### d. Summer cooling estimation

Linear regression was used to reconstruct the regional August–September  $T_{\text{dev}}$  over the period 1620–2014. The skill of the regression models was verified

using split-period calibration/verification (Meko and Graybill 1995), as well as the leave-one-out and leave-five-out cross-validation methods (Michaelsen 1987). The statistics for evaluation of the regression model include Pearson's correlation coefficient  $R$ , the reduction of error (RE), the sign test (ST), the first-difference sign test (ST1), and the coefficient of efficiency (CE; Table 1). The reconstruction uncertainty is considered as the regression-based uncertainties associated with the residuals in the verification period. The uncertainty was calculated as the root-mean-square error (RMSE).

#### e. Volcanic dataset

Information regarding volcanic eruption events was obtained from the global volcanic forcing (GVF) values from Sigl et al. (2015). In total, 27 relatively large eruptions ( $\text{GVF} < -1$ ) that occurred in the NH mid–high latitudes and tropics since 1620 were used in this study (Table 2). The 27 events include 14 tropical eruptions and 13 extratropical eruptions. The GVF was estimated from the reconstruction of volcanic aerosol deposition since early Roman times for both polar ice sheets. The main difference between this reconstruction and previous ones is that this reconstruction performed a time-scale revision before 1257 and added new high-resolution, ice-core sulfur measurements. The NH mid- to high-latitude eruptions were claimed using sulfate deposition from the Greenland ice cores, while tropical eruptions were

TABLE 1. Statistics of calibration and verification for the regression models.

Calibration						Split-period verification					
Period	$r$	$R^2$	$R^2_{\text{adj}}$	$F$	DW	Period	$r$	RE	ST	ST1	CE
1956–85	0.71	0.51	0.49	29.2	1.6	1986–2014	0.81	0.60	23+/6–	23+/5–	0.59
1986–2014	0.81	0.66	0.65	52.7	1.9	1956–85	0.71	0.45	23+/7–	21+/8–	0.42
1956–2014	0.75	0.57	0.56	75.1	1.8	—	—	—	—	—	—
									Leave-one-out verification		
						1956–2014	0.75	0.51	44+/15–	45+/13–	—
									Leave-five-out verification		
						1956–2014	0.73	0.52	43+/16–	45+/13–	—

confirmed based on synchronous sulfate deposition on both polar ice sheets (Sigl et al. 2015).

#### f. El Niño events

We considered El Niño events that occurred since 1620. This information stems from Table 2 in the paper of Brönnimann et al. (2007), which was based on a number of indices and datasets, including multiple proxy records. This El Niño dataset covers the period of 1500–2003, and three subperiods Reconstruction1 (REC1) (1500–1705), Reconstruction2 (REC2) (1706–1879), and Instrument (INS) (1880–2003) were defined. El Niño events that occurred in the period of 1880–2003 were identified using an observational sea surface temperature (SST) data (ERSST, version 2, data; Brönnimann et al. 2007). Information on El Niño events in the REC1 and REC2 periods were obtained from multisource proxy reconstructions. The El Niño events in the REC2 period were confirmed based on more proxy data, and the associated information has a higher quality than that in the REC1 period. Based on the long ENSO events chronology, Brönnimann et al. (2007) found a stationary relationship between ENSO and the European

climate over a long historical period. Importantly, the volcanic forcing series, ENSO reconstructions, and TP temperature reconstruction used in the study are all data independent.

### 3. Results

Growth-response analysis showed that MXD\_GD correlates significantly with the regional  $T_{\text{dev}}$  during August and September (Fig. 3). Further analysis considering individual station records indicates that the MXD\_GD series correlates significantly ( $P < 0.001$ ) with the August–September  $T_{\text{dev}}$  at 69 of the 79 stations (Fig. 1). The correlation coefficients between MXD\_GD and the regional August–September  $T_{\text{dev}}$  from 79-, 69-, and 62-station means are 0.71 [effective degrees of freedom (edf) = 58,  $P < 0.001$ ], 0.74 (edf = 58,  $P < 0.001$ ), and 0.75 (edf = 58,  $P < 0.001$ ), respectively, over the instrumental period of 1956–2014. We used the 62-station average based on the similarity of the spatial coverage to that of the MXD network (dotted red box in Fig. 1). Sensitivity tests (not shown) suggest that averaging over a

TABLE 2. Volcanic forcing information used in this study. The years marked in bold font indicate eruptions without El Niño associations, while the other years denote eruptions with a subsequent El Niño event. All the event years used here have a value of GVF < -1.

Event year_tropics	GVF ( $\text{W m}^{-2}$ )	Event year_NH mid-high latitudes	GVF ( $\text{W m}^{-2}$ )
<b>1641</b>	-11.84	<b>1637</b>	-1.00
1673	-3.11	<b>1646</b>	-1.91
<b>1693</b>	-1.38	<b>1654</b>	-1.48
<b>1695</b>	-10.24	<b>1667</b>	-2.33
<b>1762</b>	-3.52	<b>1729</b>	-3.17
<b>1809</b>	-12.01	<b>1739</b>	-2.36
1815	-17.20	1766	-1.41
1832	-6.46	1783	-15.49
<b>1836</b>	-6.57	<b>1846</b>	-1.12
<b>1862</b>	-4.03	<b>1908</b>	-1.18
<b>1884</b>	-5.84	<b>1912</b>	-3.26
<b>1943</b>	-1.76	<b>1925</b>	-1.03
<b>1964</b>	-3.75	<b>1926</b>	-1.79
1991	-6.49	—	—
—	Mean (-6.70)	—	Mean (-2.89)



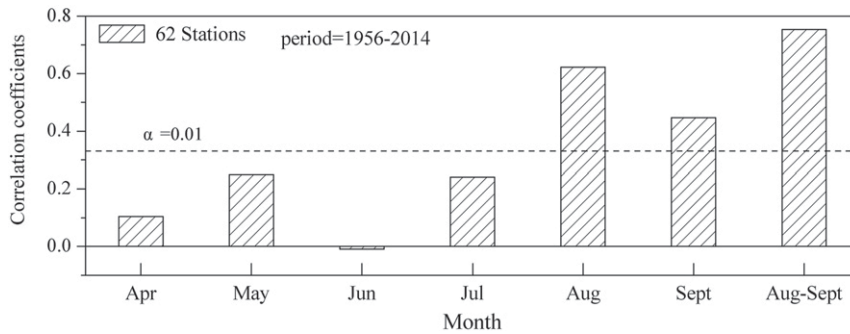


FIG. 3. Growth–response relationships of the regional MXD\_GD series with regional  $T_{\text{dev}}$  from April to September and the August–September mean.

larger station network would not affect the definition of the reconstruction target appreciably. The composite MXD\_GD series represents the regional MXD deviation relative to the preceding 5-yr mean and is a good proxy for the August–September  $T_{\text{dev}}$  on the TP from  $27^{\circ}$ – $36^{\circ}$ N to  $84^{\circ}$ – $104^{\circ}$ E ( $r_{1956-2014} = 0.75$ ,  $\text{edf} = 58$ ,  $P < 0.0001$ ; Fig. 4a).

Except for the year 1962, during which the proxy indicates colder conditions, the MXD\_GD series matches the instrumental data quite closely (Fig. 4a). The MXD outlier in 1962 is related to the coldest March–August ( $T_{\text{dev}} = -0.71^{\circ}\text{C}$ ) during 1956–2014, while the

August–September  $T_{\text{dev}}$  ( $-0.33^{\circ}\text{C}$ ) is close to the climatology. In other words, the MXD value in 1962 reflects the temperature condition in March–August but not that in August–September. These findings demonstrate that the MXD\_GD series also has the potential to indicate temperature extremes during the extended growing season (i.e., March–August) in addition to temperature extremes in August–September. Based on the MXD\_GD series, postvolcanic late-summer cooling after 27 large tropical and extratropical eruptions (i.e., events exceeding GVF values of  $-1 \text{ W m}^{-2}$ ) back to AD

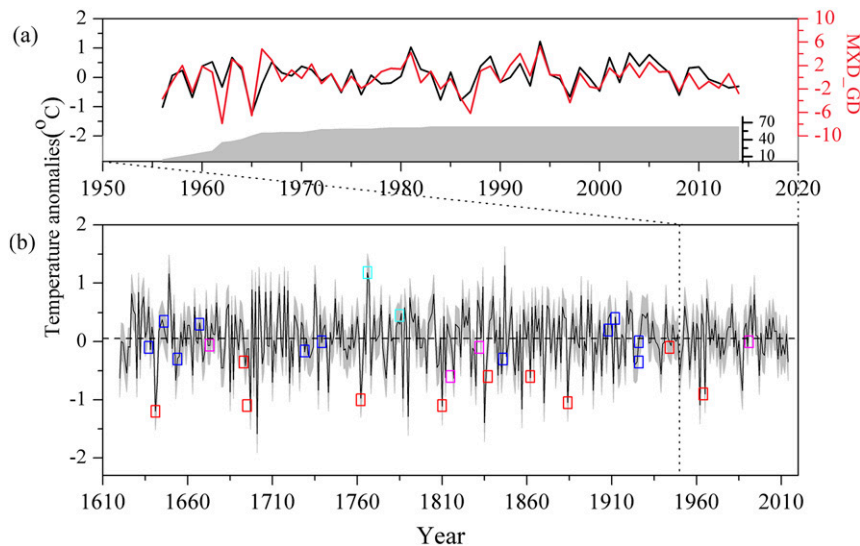


FIG. 4. The regional MXD\_GD series and August–September  $T_{\text{dev}}$  reconstruction. (a) Comparison between the regional MXD\_GD and the August–September  $T_{\text{dev}}$ . (b) Reconstructed August–September  $T_{\text{dev}}$  based on the regional MXD\_GD series. The inside panel in (a) indicates the changes in the number of available meteorology stations with time. The thin black line in (b) is the reconstructed August–September  $T_{\text{dev}}$  and the gray-shaded area represents the reconstruction uncertainty (i.e., reconstruction values  $\pm 1$  RMSE). The red, magenta, blue, and cyan boxes in (b) mark the tropical volcanic eruptions that were followed by an El Niño event, tropical volcanic eruptions without El Niño associations, extratropical volcanic eruptions that were followed by an El Niño event, and extratropical volcanic eruptions without El Niño associations, respectively.

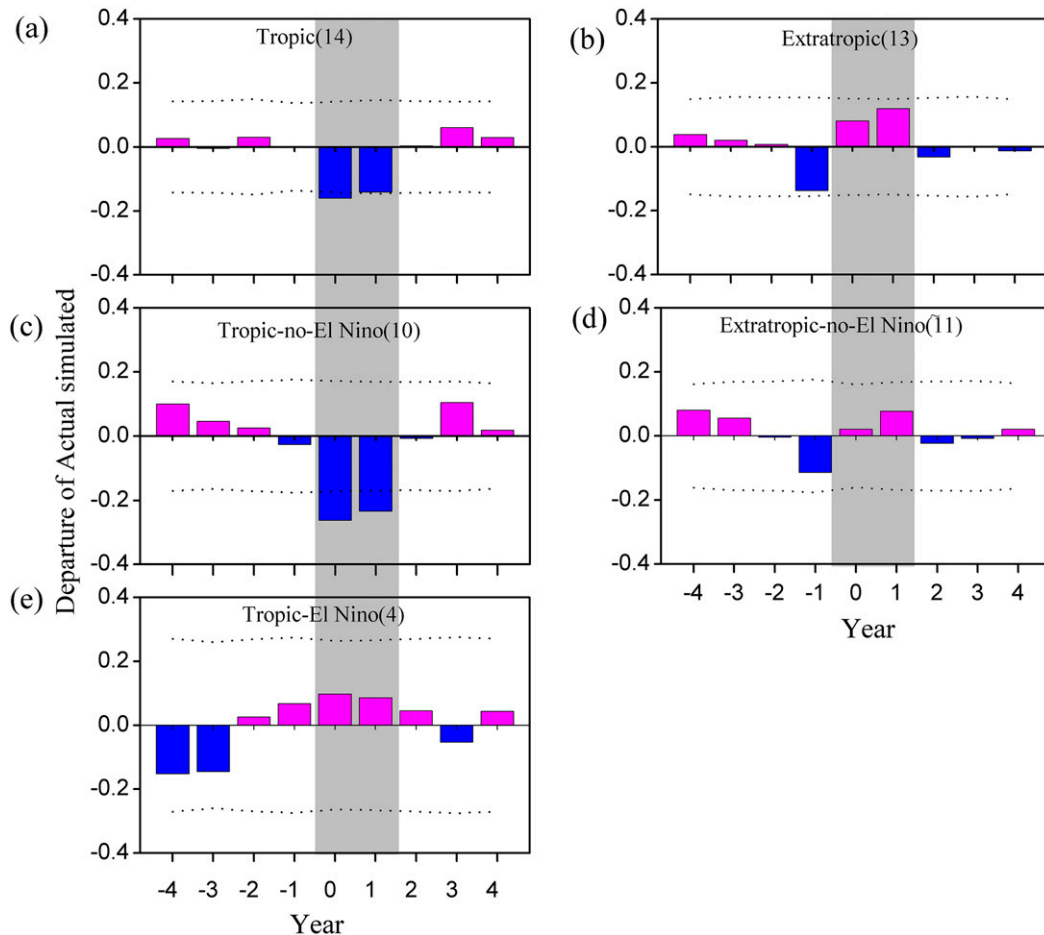


FIG. 5. SEA testing the impact of explosive volcanism on the August–September  $T_{\text{dev}}$  on the TP. SEA based on (a) 14 tropical volcanic eruptions, (b) 13 extratropical volcanic eruptions, (c) 10 tropical volcanic eruptions without a subsequent El Niño event, (d) 11 extratropical volcanic eruptions without a subsequent El Niño event, and (e) 4 tropical volcanic eruptions with El Niño associations. Information regarding volcanic eruption events were obtained from Sigl et al. (2015). Dashed lines represent the 95% confidence limits obtained by performing a Monte Carlo significance test.

1620 ( $\text{EPS} > 0.85$ ) was quantitatively reconstructed (Fig. 4b). All the associated statistics indicate a good skill of the regression model (Table 1). The  $r$ ,  $R^2$ ,  $F$ ,  $ST$ , and  $ST1$  values are significant at  $P < 0.01$ , and the positive REs and CEs suggest that the reconstructions have encouraging performances. The statistics of Durbin–Watson (DW) demonstrate no first-order autocorrelation in the model residuals.

Superposed epoch analysis (SEA) indicates that August–September cooling is stronger after tropical eruptions compared to extratropical eruptions (Fig. 5). This difference is likely related to the significantly different GVs, which are significantly larger for the tropical eruptions (Table 2). Moreover, the TP temperature changes are also variable among tropical eruptions (Fig. 4b). Among the four largest tropical eruptions ( $\text{GVF} < -10$ ), three eruptions (1641,

1695, 1809) forced cooling of the August–September  $T_{\text{dev}}$  by more than  $1.28^\circ\text{C}$ , whereas the largest eruption of Tambora in 1815 caused only a minor/modest temperature drop in 1816/17 ( $-0.25^\circ/-0.73^\circ\text{C}$ ; Fig. 4b). Tropical eruptions followed by an El Niño event produced qualitative, nonsignificant warming (Fig. 5e), opposing the significant cooling from tropical eruptions not followed by El Niño events (Fig. 5c) and dampening the composite cooling over all tropical eruptions (Fig. 5a).

#### 4. Discussion

To verify whether El Niño compensated for the postvolcanic cooling by warming the TP, we conducted a composite analysis of the gridded August–September  $T_{\text{dev}}$  considering the El Niño events that occurred

during the observational period 1961–2003 (Fig. 6). The composite spatial August–September  $T_{\text{dev}}$  field reveals a positive anomaly over a large part of the TP, demonstrating that El Niño events warmed the TP and supporting the reconstructed weakening of postvolcanic cooling effects. The possible mechanism by which ENSO warms the TP is its indirect influence on the summer monsoon. Previous studies have reported that El Niño can weaken the Indian summer monsoon, with a subsequent decrease in precipitation and accompanying drought in the regions influenced by the Indian summer monsoon (Mooley and Parthasarathy 1983; Singh and Dash 2005; Kumar et al. 2006). Summer precipitation over a large part of the TP originates from the Indian summer monsoon. Additionally, most of the annual precipitation on the TP originates from the Indian summer monsoon. Furthermore, there is a significant negative correlation between summer precipitation and summer temperature on the TP (Wang et al. 2010; Bräuning and Mantwill 2004). This means that deficient summer precipitation on the TP can induce drought and trigger high temperatures, while abundant rainfall can dampen the summer high temperature. Thus, the mechanism by which El Niño affects the TP summer temperature can be its indirect influence on the summer monsoon. The weakened Indian summer monsoon resulting from El Niño events may lead to decreased summer rainfalls and be conducive to warming summers over the TP. This supports the hypothesis that postvolcanic summer cooling on the TP can be compensated by internal phenomena (such as ENSO warm-phase events).

These results imply that a better understanding of the interannual variability of the TP late-summer temperature is needed from the perspective of both external forcing and the mediation of internal phenomena (i.e., ENSO warm phase) on the TP temperature response to external forcing. Moreover, this interaction seems to occur more often for tropical volcanic eruptions than for extratropical eruptions. Considering the eruptions with  $\text{GVF} < -1$  over the period 1620–2014, there are 4 out of 14 tropical volcanic eruptions with a subsequent El Niño event, but only 2 out of 13 extratropical eruptions have El Niño associations (Table 2).

To understand the mitigation effect of El Niño events on the response of the TP later-summer temperature to tropical volcanic eruptions, the 1815 Tambora event could be the most typical case. The reduced temperature effect of the 1815 Tambora eruption (Fig. 4) was likely triggered by the mitigating effects from the 1816 El Niño. The finding that the summer temperature in 1816 was not exceptional is also confirmed by another independent MXD chronology-based summer temperature reconstruction from central TP (Bräuning and Mantwill 2004). The cool summers in 1816 and/or 1817

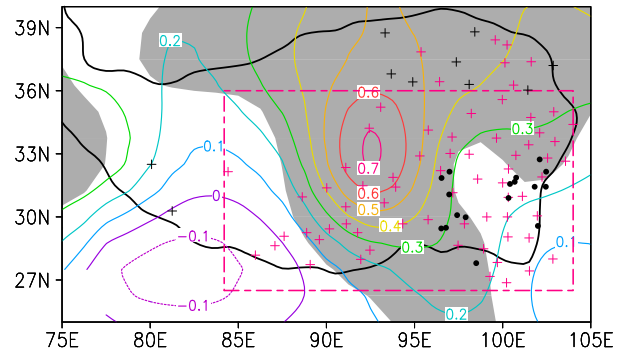


FIG. 6. Composite August–September  $T_{\text{dev}}$  ( $^{\circ}\text{C}$ ) based on El Niño years in the observational period (i.e., 1966, 1973, 1977, 1982, 1987, 1992, 1998, 2003). The gray-shaded area denotes significance at  $P < 0.05$ . The dashed-line box shows the range in which the MXD\_GD correlates significantly with the regional August–September  $T_{\text{dev}}$  ( $P < 0.05$ ). Black dots denote the locations of the MXD sampling sites, and magenta/black crosses denote the locations of meteorological stations in which the August–September  $T_{\text{dev}}$  correlates significantly ( $P < 0.05$ )/insignificantly ( $P > 0.05$ ) with the MXD series.

after the Tambora eruption in April 1815 have also been found in other tree-ring studies on the TP (Liang et al. 2008; Bräuning and Mantwill 2004; Wang et al. 2010; Fan et al. 2009; Li et al. 2015). However, the magnitude of summer cooling in 1816/17 resulting from the Tambora eruption in 1815 is obviously less than that in 1810, driven by an unknown tropical eruption in 1809 (Bräuning and Mantwill 2004; Wang et al. 2010; Fan et al. 2009; Li et al. 2015). This pattern is coherent with our finding, but it is in contrast to the NH records (Briffa et al. 1998; Sigl et al. 2015). In particular, the greatest magnitude of summer cooling identified in the NH record since 1620, which occurred in 1816 (Briffa et al. 1998; Sigl et al. 2015), cannot be found in almost any tree-ring-based summer temperature reconstruction on the TP (Bräuning and Mantwill 2004; Liang et al. 2008; Gou et al. 2008; Liu et al. 2009; Fan et al. 2009; Wang et al. 2010; Yang et al. 2010; Zhu et al. 2011; Li et al. 2012; Li et al. 2015; Yin et al. 2015). This result supports the hypothesis that the TP summer cooling driven by the 1815 Tambora eruption had been mitigated by another factor. These results imply that although volcanic eruptions cause cooling in general, the particular regional response can be masked by other processes that may be independent of or even related to volcanism.

## 5. Conclusions

Our results indicate that the effects of tropical eruptions on the TP are significantly greater than those of extratropical eruptions. Moreover, tropical eruptions followed by an El Niño event produced qualitative,



nonsignificant warming, opposing significant cooling from tropical eruptions not followed by El Niño events and dampening the composite cooling from overall tropical eruptions. Based on 27 events, including 14 tropical eruptions and 13 extratropical eruptions, over the period 1620–2014, the average magnitude change driven by large tropical eruptions without a subsequent El Niño event is approximately  $-0.48^{\circ} \pm 0.19^{\circ}\text{C}$ , while that caused by events with an El Niño association is approximately  $0.23^{\circ} \pm 0.16^{\circ}\text{C}$ . These results imply a mediation effect of El Niño events on the TP temperature response to tropical eruptions. A possible mechanism of the El Niño mediation of the response of the TP temperature to volcanic eruptions can be its indirect influence on the summer monsoon. Specifically, El Niño can weaken the Indian summer monsoon, in which a subsequent decrease in precipitation and accompanying drought occurs in the regions influenced by the Indian summer monsoon. Summer precipitation over a large part of the TP, where most of the regional precipitation occurs in summer, originates from the Indian summer monsoon. Therefore, there is a significant anticorrelation between summer precipitation and temperature on the TP. Thus, deficient summer precipitation on the TP can induce drought and trigger high temperatures, while abundant rainfall can dampen the summer high temperature. The reduced temperature effect in response to the strong tropical eruption of Tambora in April 1815 is perhaps a typical case for the TP.

*Acknowledgments.* This research was supported by the National Key R&D Program of China (2016YFA0600404), the National Natural Science Foundation of China (Grants 41471035, 41101043, and 41405054). We thank Dr. Hongbin Liu for assistance in MXD measurement, and also greatly appreciate the Laboratory for Climate Studies, China Meteorological Administration for allowing us to use the densitometric devices. We thank the National Meteorological Information Center of China Meteorological Administration for making meteorological station data available. Jianping Duan acknowledges support from the Alexander von Humboldt Foundation. Lun Li was also supported from the Basic Scientific Research and Operation Foundation of CAMS (2016Y001). Jürg Luterbacher was supported from the German Science Foundation (DFG) project AFICHE and the Belmont Forum and JPI-Climate Collaborative Research Action “INTEGRATE: An integrated data-model study of interactions between tropical monsoons and extra-tropical climate variability and extremes.” The meteorological stations data used in this study are available for application at China Meteorological Data Sharing Service System ([http://data.cma.cn/data/cdcdetail/dataCode/SURF\\_CLI\\_CHN\\_MUL\\_MON.html](http://data.cma.cn/data/cdcdetail/dataCode/SURF_CLI_CHN_MUL_MON.html)). The

regional tree-ring series and temperature reconstruction will be archived at the NOAA paleodataset. Additional data related to this paper may be requested from the corresponding author.

## REFERENCES

- Anchukaitis, K. J., B. M. Buckley, E. R. Cook, B. I. Cook, R. D. D’Arrigo, and C. M. Ammann, 2010: Influence of volcanic eruptions on the climate of the Asian monsoon region. *Geophys. Res. Lett.*, **37**, L22703, <https://doi.org/10.1029/2010GL044843>.
- Bräuning, A., and B. Mantwill, 2004: Summer temperature and summer monsoon history on the Tibetan plateau during the last 400 years recorded by tree rings. *Geophys. Res. Lett.*, **31**, L24205, <https://doi.org/10.1029/2004GL020793>.
- Briffa, K. R., P. D. Jones, and F. H. Schweingruber, 1988: Summer temperature patterns over Europe: A reconstruction from 1750 A.D. based on maximum latewood density indexes of conifers. *Quat. Res.*, **30**, 36–52, [https://doi.org/10.1016/0033-5894\(88\)90086-5](https://doi.org/10.1016/0033-5894(88)90086-5).
- , —, —, and T. J. Osborn, 1998: Influence of volcanic eruptions on Northern Hemisphere summer temperature over the past 600 years. *Nature*, **393**, 450–455, <https://doi.org/10.1038/30943>.
- Brönnimann, S., E. Xoplaki, C. Casty, A. Pauling, and J. Luterbacher, 2007: ENSO influence on Europe during the last centuries. *Climate Dyn.*, **28**, 181–197, <https://doi.org/10.1007/s00382-006-0175-z>.
- Büntgen, U., and Coauthors, 2015: Tree-ring amplification of the early nineteenth-century summer cooling in central Europe. *J. Climate*, **28**, 5272–5288, <https://doi.org/10.1175/JCLI-D-14-00673.1>.
- , and Coauthors, 2016: Cooling and societal change during the Late Antique Little Ice Age from 536 to around 660 AD. *Nat. Geosci.*, **9**, 231–236, <https://doi.org/10.1038/ngeo2652>.
- Cook, E. R., and P. J. Krusic, 2005: ARSTAN: A tree-ring standardization program based on detrending and autoregressive time series modeling, with interactive graphics. Lamont-Doherty Earth Observatory, Columbia University, <https://www.ldeo.columbia.edu/tree-ring-laboratory/resources/software>.
- , —, K. J. Anchukaitis, B. M. Buckley, T. Nakatsuka, and M. Sano, 2013: Tree-ring reconstructed summer temperature anomalies for temperate East Asia since 800 C.E. *Climate Dyn.*, **41**, 2957–2972, <https://doi.org/10.1007/s00382-012-1611-x>.
- D’Arrigo, R., R. Wilson, and A. Tudhope, 2009: The impact of volcanic forcing on tropical temperatures during the past four centuries. *Nat. Geosci.*, **2**, 51–56, <https://doi.org/10.1038/ngeo393>.
- Duan, J., and Q.-B. Zhang, 2014: A 449 year warm season temperature reconstruction in the southeastern Tibetan Plateau and its relation to solar activity. *J. Geophys. Res. Atmos.*, **119**, 11 578–11 592, <https://doi.org/10.1002/2014JD022422>.
- , L. Wang, L. Li, and K. Chen, 2010: Temperature variability since AD 1837 inferred from tree-ring maximum density of *Abies fabri* on Gongga Mountain, China. *Chin. Sci. Bull.*, **55**, 3015–3022, <https://doi.org/10.1007/s11434-010-3182-8>.
- , L. Li, and Y. Fang, 2015: Seasonal spatial heterogeneity of warming rates on the Tibetan Plateau over the past 30 years. *Sci. Rep.*, **5**, 11725, <https://doi.org/10.1038/srep11725>.
- , and Coauthors, 2017: Weakening of annual temperature cycle over the Tibetan Plateau since the 1870s. *Nat. Commun.*, **8**, 14008, <https://doi.org/10.1038/ncomms14008>.

- Esper, J., U. Büntgen, J. Luterbacher, and P. J. Krusic, 2013a: Testing the hypothesis of post-volcanic missing rings in temperature sensitive dendrochronological data. *Dendrochronologia*, **31**, 216–222, <https://doi.org/10.1016/j.dendro.2012.11.002>.
- , L. Schneider, P. J. Krusic, J. Luterbacher, U. Büntgen, M. Timonen, F. Sirocko, and E. Zorita, 2013b: European summer temperature response to annually dated volcanic eruptions over the past nine centuries. *Bull. Volcanol.*, **75**, 736–750, <https://doi.org/10.1007/s00445-013-0736-z>.
- , —, J. E. Smerdon, B. R. Schöne, and U. Büntgen, 2015: Signals and memory in tree-ring width and density data. *Dendrochronologia*, **35**, 62–70, <https://doi.org/10.1016/j.dendro.2015.07.001>.
- Fan, Z.-X., A. Bräuning, B. Yang, and K.-F. Cao, 2009: Tree ring density-based summer temperature reconstruction for the central Hengduan Mountains in southern China. *Global Planet. Change*, **65**, 1–11, <https://doi.org/10.1016/j.gloplacha.2008.10.001>.
- Frank, D., U. Büntgen, R. Böhm, M. Maugeri, and J. Esper, 2007: Warmer early instrumental measurements versus colder reconstructed temperatures: Shooting at a moving target. *Quat. Sci. Rev.*, **26**, 3298–3310, <https://doi.org/10.1016/j.quascirev.2007.08.002>.
- Gou, X., J. Peng, F. Chen, M. Yang, D. F. Levia, and J. Li, 2008: A dendrochronological analysis of maximum summer half-year temperature variations over the past 700 years on the north-eastern Tibetan Plateau. *Theor. Appl. Climatol.*, **93**, 195–206, <https://doi.org/10.1007/s00704-007-0336-y>.
- Holmes, R. L., 1983: Computer-assisted quality control in tree-ring dating and measurement. *Tree-Ring Bull.*, **43**, 69–78.
- Jones, P. D., D. H. Lister, T. J. Osborn, C. Harpham, M. Salmon, and C. P. Morice, 2012: Hemispheric and large-scale land-surface air temperature variations: An extensive revision and an update to 2010. *J. Geophys. Res.*, **117**, D05127, <https://doi.org/10.1029/2011JD017139>.
- Kumar, K. K., B. Rajagopalan, and M. A. Cane, 1999: On the weakening relationship between the Indian monsoon and ENSO. *Science*, **284**, 2156–2159, <https://doi.org/10.1126/science.284.5423.2156>.
- , —, M. Hoerling, G. Bates, and M. Cane, 2006: Unraveling the mystery of Indian monsoon failure during El Niño. *Science*, **314**, 115–119, <https://doi.org/10.1126/science.1131152>.
- Li, M.-Y., L. Wang, Z.-X. Fan, and C.-C. Shen, 2015: Tree-ring density inferred late summer temperature variability over the past three centuries in the Gaoligong Mountains, southeastern Tibetan Plateau. *Palaeogeogr. Palaeoclimatol. Palaeoecol.*, **422**, 57–64, <https://doi.org/10.1016/j.palaeo.2015.01.003>.
- Li, Z.-S., Q.-B. Zhang, and K. Ma, 2012: Tree-ring reconstruction of summer temperature for A.D. 1475–2003 in the central Hengduan Mountains, northwestern Yunnan, China. *Climatic Change*, **110**, 455–467, <https://doi.org/10.1007/s10584-011-0111-z>.
- Liang, E., X. Shao, and N. Qin, 2008: Tree-ring based summer temperature reconstruction for the source region of the Yangtze River on the Tibetan Plateau. *Global Planet. Change*, **61**, 313–320, <https://doi.org/10.1016/j.gloplacha.2007.10.008>.
- Liu, Y., Z. An, H. W. Linderholm, D. Chen, H. Song, Q. Cai, J. Sun, and H. Tian, 2009: Annual temperatures during the last 2485 years in the mid-eastern Tibetan Plateau inferred from tree rings. *Sci. China Ser.*, **52D**, 348–359, <https://doi.org/10.1007/s11430-009-0025-z>.
- Luterbacher, J., and C. Pfister, 2015: The year without a summer. *Nat. Geosci.*, **8**, 246–248, <https://doi.org/10.1038/ngeo2404>.
- , and Coauthors, 2016: European summer temperatures since Roman times. *Environ. Res. Lett.*, **11**, 024001, <https://doi.org/10.1088/1748-9326/11/2/024001>.
- Meko, D., and D. A. Graybill, 1995: Tree-ring reconstruction of upper Gila River discharge. *J. Amer. Water Resour. Assoc.*, **31**, 605–616, <https://doi.org/10.1111/j.1752-1688.1995.tb03388.x>.
- Michaelsen, J., 1987: Cross-validation in statistical climate forecast models. *J. Climate Appl. Meteor.*, **26**, 1589–1600, [https://doi.org/10.1175/1520-0450\(1987\)026<1589:CVISCF>2.0.CO;2](https://doi.org/10.1175/1520-0450(1987)026<1589:CVISCF>2.0.CO;2).
- Mooley, D. A., and B. Parthasarathy, 1983: Indian summer monsoon and El Niño. *Pure Appl. Geophys.*, **121**, 339–352, <https://doi.org/10.1007/BF02590143>.
- Oppenheimer, C., 2003: Climatic, environmental and human consequences of the largest known historic eruption: Tambora volcano (Indonesia) 1815. *Prog. Phys. Geogr.*, **27**, 230–259, <https://doi.org/10.1191/0309133303pp379ra>.
- Privalsky, V. E., and D. T. Jensen, 1995: Assessment of the influence of ENSO on annual global air temperatures. *Dyn. Atmos. Oceans*, **22**, 161–178, [https://doi.org/10.1016/0377-0265\(94\)00400-Q](https://doi.org/10.1016/0377-0265(94)00400-Q).
- Robock, A., 2000: Volcanic eruptions and climate. *Rev. Geophys.*, **38**, 191–219, <https://doi.org/10.1029/1998RG000054>; Corrigendum, **45**, RG3005, <https://doi.org/10.1029/2007RG000232>.
- Sato, T., 2009: Influences of subtropical jet and Tibetan Plateau on precipitation pattern in Asia: Insights from regional climate modeling. *Quat. Int.*, **194**, 148–158, <https://doi.org/10.1016/j.quaint.2008.07.008>.
- Schneider, L., J. E. Smerdon, F. Pretis, C. Hartl-Meier, and J. Esper, 2017: A new archive of large volcanic events over the past millennium derived from reconstructed summer temperatures. *Environ. Res. Lett.*, **12**, 094005, <https://doi.org/10.1088/1748-9326/aa7a1b>; Corrigendum, **12**, 119501, <https://doi.org/10.1088/1748-9326/aa9426>.
- Schweingruber, F. H., T. Bartholin, E. Schär, and K. R. Briffa, 1988: Radiodensitometric-dendroclimatological conifer chronologies from Lapland (Scandinavia) and the Alps (Switzerland). *Boreas*, **17**, 559–566, <https://doi.org/10.1111/j.1502-3885.1988.tb00569.x>.
- , D. Eckstein, F. Serre-Bachet, and O. U. Bräker, 1990: Identification, presentation and interpretation of event years and pointer years in dendrochronology. *Dendrochronologia*, **8**, 9–38.
- , K. R. Briffa, and P. D. Jones, 1991: Yearly maps of summer temperatures in western Europe from A.D. 1750 to 1975 and western North America from 1600 to 1982: Results of a radiodensitometric study on tree rings. *Vegetatio*, **92**, 5–71, <https://doi.org/10.1007/BF00047132>.
- Sigl, M., and Coauthors, 2015: Timing and climate forcing of volcanic eruptions for the past 2,500 years. *Nature*, **523**, 543–549, <https://doi.org/10.1038/nature14565>.
- Singh, G. P., and S. K. Dash, 2005: Atmospheric circulation characteristics during some El-Niño years in relation to Indian summer monsoon rainfall. *Theor. Appl. Climatol.*, **81**, 113–120, <https://doi.org/10.1007/s00704-004-0090-3>.
- Stine, A. R., and P. Huybers, 2014: Arctic tree rings as recorders of variations in light availability. *Nat. Commun.*, **5**, 3836, <https://doi.org/10.1038/ncomms4836>.
- Stoffel, M., and Coauthors, 2015: Estimates of volcanic-induced cooling in the Northern Hemisphere over the past 1,500 years. *Nat. Geosci.*, **8**, 784–788, <https://doi.org/10.1038/ngeo2526>.
- Stothers, R. B., 1984: The great Tambora eruption in 1815 and its aftermath. *Science*, **224**, 1191–1198, <https://doi.org/10.1126/science.224.4654.1191>.
- Wang, L., J. Duan, J. Chen, L. Huang, and X. Shao, 2010: Temperature reconstruction from tree-ring maximum density of Balfour spruce in eastern Tibet, China. *Int. J. Climatol.*, **30**, 972–979, <https://doi.org/10.1002/joc.2000>.

- Wang, N., L. G. Thompson, M. E. Davis, E. Mosley-Thompson, Y. Tandong, and P. Jianchen, 2003: Influence of variations in NAO and SO on air temperature over the northern Tibetan Plateau as recorded by  $\delta^{18}\text{O}$  in the Malan ice core. *Geophys. Res. Lett.*, **30**, 2167, <https://doi.org/10.1029/2003GL018188>.
- Wigley, T. M. L., K. R. Briffa, and P. D. Jones, 1984: On the average value of correlated time-series, with applications in dendroclimatology and hydrometeorology. *J. Climate Appl. Meteor.*, **23**, 201–213, [https://doi.org/10.1175/1520-0450\(1984\)023<0201:OTAVOC>2.0.CO;2](https://doi.org/10.1175/1520-0450(1984)023<0201:OTAVOC>2.0.CO;2).
- Yang, B., X. Kang, A. Bräuning, J. Liu, C. Qin, and J. Liu, 2010: A 622-year regional temperature history of southeast Tibet derived from tree rings. *Holocene*, **20**, 181–190, <https://doi.org/10.1177/0959683609350388>.
- Yao, T., and Coauthors, 2012: Different glacier status with atmospheric circulations in Tibetan Plateau and surroundings. *Nat. Climate Change*, **2**, 663–667, <https://doi.org/10.1038/nclimate1580>.
- Yin, H., H. Liu, H. W. Linderholm, and Y. Sun, 2015: Tree ring density-based warm-season temperature reconstruction since A.D. 1610 in the eastern Tibetan Plateau. *Palaeogeogr. Palaeoclimatol. Palaeoecol.*, **426**, 112–120, <https://doi.org/10.1016/j.palaeo.2015.03.003>.
- Yin, Z., Z. Lin, and X. Zhao, 2000: Temperature anomalies in central and eastern Tibetan Plateau in relation to general circulation patterns during 1951–1993. *Int. J. Climatol.*, **20**, 1431–1449, [https://doi.org/10.1002/1097-0088\(200010\)20:12<1431::AID-JOC551>3.0.CO;2-J](https://doi.org/10.1002/1097-0088(200010)20:12<1431::AID-JOC551>3.0.CO;2-J).
- Zhu, H.-F., X.-M. Shao, Z.-Y. Yin, P. Xu, Y. Xu, and H. Tian, 2011: August temperature variability in the southeastern Tibetan Plateau since AD 1385 inferred from tree rings. *Palaeogeogr. Palaeoclimatol. Palaeoecol.*, **305**, 84–92, <https://doi.org/10.1016/j.palaeo.2011.02.017>.